

1 **Bayesian Data Fusion for water table interpolation: incorporating a hydrogeological**
2 **conceptual model in kriging**

3 Luk Peeters^{(1)*}, Dominique Fasbender⁽²⁾, Okke Batelaan^(1,3), Alain Dassargues^(1,4)

4

5 (1) Dept. Earth & Environmental Sciences, KULeuven. Celestijnenlaan 200E bus 2408, 3001
6 Heverlee, Belgium

7 (2) Institut National de la Recherche Scientifique, Centre Eau, Terre et Environnement. 490
8 de la Couronne, G1K 9A9 Quebec City, QC, Canada.

9 (3) Dept. of Hydrology and Hydraulic Engineering Vrije Universiteit Brussel, Pleinlaan 2,
10 1050 Brussels, Belgium

11 (4) Hydrogéologie et Géologie de l'Environnement, Dpt ArGenCo (Architecture, Geology,
12 Environment and Constructions) Université de Liège, B.52/3 Sart-Tilman, 4000 Liège,
13 Belgium

* Corresponding Author: email: luk.peeters@csiro.com

14 **Abstract**

15 The creation of a contour map of the water table in an unconfined aquifer based on head
16 measurements is often the first step in any hydrogeological study. Geostatistical interpolation
17 methods (e.g. kriging) may provide exact interpolated groundwater levels at the measurement
18 locations, but often fail to represent the hydrogeological flow system. A physically based,
19 numerical groundwater model with spatially variable parameters and inputs is more adequate
20 in representing a flow system. Due to the difficulty in parameterization and solving the
21 inverse problem however, an often considerable difference between calculated and observed
22 heads will remain.

23 In this study the water table interpolation methodology presented by Fasbender *et al.* (2008),
24 in which the results of a kriging interpolation are combined with information from a drainage
25 network and a Digital Elevation Model (DEM), using the Bayesian Data Fusion framework
26 (Bogaert and Fasbender, 2007), is extended to incorporate information from a tuned analytic
27 element groundwater model. The resulting interpolation is exact at the measurement locations
28 while the shape of the head contours is in accordance with the conceptual information
29 incorporated in the groundwater flow model.

30 The Bayesian Data Fusion methodology is applied to a regional, unconfined aquifer in Central
31 Belgium. A cross-validation procedure shows that the predictive capability of the
32 interpolation at unmeasured locations benefits from the Bayesian Data Fusion of the three
33 data sources (kriging, DEM and groundwater model), compared to the individual data sources
34 or any combination of two data sources.

35 1. Introduction

36 A head contour map provides information about the flow direction and gradient of an aquifer
37 system and, in the case of an unconfined aquifer, about the depth of the water table. Such a
38 contour map is used as starting point to gain insight in the groundwater flow system, to
39 evaluate migration of pollutants, to assess vulnerability of an aquifer and to create conceptual
40 hydrogeological models.

41 Head observation data however, are often scarce and irregularly distributed over a study area.
42 To obtain a head contour map based on these data a number of approaches are available,
43 ranging in complexity from manually drawing contour lines over interpolation to groundwater
44 modeling.

45 The most straight forward method to create a water table map is to manually create contours
46 based on observation data. This method has the distinct advantage of directly incorporating
47 expert knowledge about the hydrogeological system under study (Kresic, 2006). A major
48 drawback of manual interpolation is the inherent subjectivity of the method since each expert
49 will have a personal interpretation of the available data and hydrogeological information. A
50 second drawback is the time consuming nature of the method, especially for large regions and
51 datasets.

52 The other side of the spectrum of available methods to produce comprehensive and reliable
53 water table maps, is physically based, numerical groundwater modeling with spatially
54 distributed parameter and input values. Based on the hydrogeological information
55 implemented through the conceptual model, a piezometric map is produced in accordance
56 with the governing groundwater flow equations and mass-balance constraints. The major
57 disadvantage of creating such a numerical model to obtain a head contour map is the large
58 amount of hydrogeological data required and the time and the effort needed to create and
59 calibrate the model, while, even with a calibrated model, a certain mismatch remains between

60 observed and simulated heads. By increasing the number of parameters and applying
61 optimization algorithms, it is possible to produce one or even several groundwater models
62 without residuals between observed and simulated heads. The decrease in model error is
63 however mostly accompanied by a loss of generalization of the model, the ability to
64 adequately simulate head at unmeasured locations (Hill & Tiedeman, 2007). Numerical
65 groundwater models are therefore seldom created for the sole purpose of creating a
66 groundwater contour map. On the contrary, a contour map is often essential in the
67 conceptualization of boundary conditions for a groundwater model (Reilly, 2001).

68 To create a water table map from groundwater level observations, a wide variety of
69 interpolation techniques is available, including radial basis functions, inverse distance
70 weighting (IDW) and different kriging variants. Recent applications of these methods in the
71 context of water table mapping can be found in Procter *et al.* (2006), Taany *et al.* (2009) and
72 Sun *et al.* (2009). While these methods honor the data at the measurement locations, they
73 suffer from the same drawbacks, namely an inadequate representation of the flow system and
74 the occurrence of interpolation artifacts. The inadequate representation of the flow system can
75 be manifested through groundwater levels being interpolated above topography, lacking of
76 flow convergence near draining rivers or the occurrence of isolated groundwater level
77 depressions in the absence of groundwater extractions. While these isolated groundwater level
78 depressions can occur naturally, especially in areas with high evapotranspiration rates, in
79 humid and temperate climates however, isolated groundwater level depressions generally are
80 only linked to groundwater abstraction.

81 Depending on the method chosen and the implementation of the method, interpolation
82 artifacts can cause both too much smoothing of the surface and abrupt changes in the
83 interpolated surface. Additionally, isolated observations can be overemphasized in the

84 interpolation process so that the importance of these observations in the overall interpolation
85 is disproportionately large.

86 In order to overcome these drawbacks several authors proposed incorporating auxiliary data
87 in the interpolation process. Kresic (2006) documents the widely used technique of including
88 dummy points in the interpolation. These artificial points can represent for instance a river
89 stage and are included in the interpolation process as extra observations. In doing so the
90 interpolation can be guided as to incorporate a drainage system. Buchanan and Triantafilis
91 (2009) improved IDW and ordinary kriging interpolations of groundwater depth using a
92 multiple linear regression of high-resolution geophysical measurements, morphometric
93 information and observed groundwater levels.

94 Since in unconfined aquifers groundwater levels are often related to topography (Haitjema
95 and Mitchell-Bruker, 2005) and digital elevation models (DEM) are readily available, DEM
96 information can often be used as auxiliary variable in water table interpolation. Desbarats et
97 al. (2002) provides a good overview of different methodologies of incorporating DEM
98 information in a kriging interpolation. Another approach of improving water table
99 interpolation is to incorporate groundwater level calculations based on groundwater flow
100 equations. The groundwater depth calculated using a linear relationship between groundwater
101 depth and a DEM-derived quantity, the topographic index, as implemented in TOPMODEL,
102 is used by Desbarats et al. (2002) as external drift in kriging groundwater depths in Ontario,
103 Canada. Tonkin and Larson (2002) incorporate the Theis equation in the calculation of the
104 drift term in kriging in order to account for the effect of pumping on groundwater elevation.
105 Karanovic *et al.* (2009) extend this methodology by using drift terms derived from an
106 analytical element method to include both linear and circular sinks and sources. Rivest et al.
107 (2008) adopts a similar approach where the results of a numerical groundwater model are
108 used as external drift in the interpolation of a groundwater head field in an earthen dam. Linde

109 et al. (2007) uses a Bayesian framework to combine self-potential measurements with
110 groundwater level observations to estimate the water table elevation.

111 The Bayesian Data Fusion framework was recently used by Fasbender et al. (2008) to
112 combine a kriged groundwater contour map with information from a DEM and river network.
113 An empirically derived relationship between groundwater depth and the topography based
114 penalized distance to the river network, is combined with an ordinary kriging of head
115 observation data. Compared to ordinary kriging and co-kriging, the resulting interpolation
116 showed an improved accuracy. Additionally, the hydrogeological reality was more closely
117 reflected in the interpolated surface, since groundwater flow converged towards draining
118 rivers and interpolated head was maintained below the topography.

119 In this study the Bayesian Data Fusion framework for groundwater head interpolation is
120 extended to implicitly incorporate conceptual hydrogeological information by using a solution
121 to the groundwater flow equations under simplified boundary conditions, obtained by the
122 analytic element method.

123 The methodology is applied to a regional, unconfined, sandy aquifer in Belgium. The
124 performance of the interpolation in terms of predictive capability is assessed using a ‘leave-
125 one-out’ cross-validation procedure in which the predictive capability of the individual data
126 sources (kriging, empirical depth-distance relationship or groundwater model) and any
127 combination of two data sources is compared to an interpolation using all three data sources.

128 **2. Interpolation Methodology**

129 The goal of any interpolation is to estimate a variable of interest Z_0 at an unsampled location
130 \mathbf{x}_0 based on observations $\mathbf{z}_S = \{z_1, z_2, \dots, z_m\}$ at locations $\mathbf{x}_S = \{x_1, x_2, \dots, x_m\}$. In addition to the
131 direct observations of the variable of interest, indirect observations $\mathbf{y} = \{y_0, y_1, \dots, y_n\}$ of
132 secondary data sources \mathbf{Y} at locations $\{x_0, x_1, \dots, x_n\}$ can be used to refine in the interpolation.
133 In order to apply such a fusion of data, Bayesian approaches have shown to provide good

134 results in various fields like image processing, remote sensing and environmental modeling.
 135 An overview of these applications can be found in Bogaert and Fasbender (2007) and
 136 Fasbender *et al.* (2008). The Ensemble Kalman Filter data assimilation technique, which is
 137 widely applied in atmospheric science (Ehrendorfer, 2007), can be considered to be a special
 138 case of Empirical Bayesian Data Fusion (Cressie and Wikle, 2002).
 139 Within the Bayesian Data Fusion framework, the interpolation methodology seeks the
 140 posterior probability density function (pdf) $f(z_0|y_0)$, the pdf of variable z at unsampled location
 141 \mathbf{x}_0 , given y_0 , the secondary information at location \mathbf{x}_0 . In this study the secondary information
 142 consists of a kriging estimate at \mathbf{x}_0 based on observations $\mathbf{z}_S = \{z_1, z_2, \dots, z_m\}$ at locations $\mathbf{x}_S =$
 143 $\{\mathbf{x}_1, \mathbf{x}_2, \dots, \mathbf{x}_m\}$, an estimate of z_0 by an empirical depth-distance relationship and an estimate z_0
 144 by an analytical element groundwater model. This section describes the fusion of the different
 145 data sources while the details of the individual data sources, kriging, depth-distance
 146 relationship and analytical element method will be discussed in section 3.
 147 The m secondary data sources at \mathbf{x}_0 , $\mathbf{Y}_0 = (Y_{0,1}, \dots, Y_{0,m})'$, are related to the variable of interest,
 148 \mathbf{Z}_0 , through an error term \mathbf{E}_0 :

$$149 \quad Y_{0,j} = Z_0 + E_{0,j} \quad \forall j = 1, \dots, m$$

150 Under the assumption of mutual independence of the secondary data sources conditionally to
 151 the variable \mathbf{Z}_0 , Bogaert and Fasbender (2007) show that the posterior pdf $f(z_0|y_0)$ can be
 152 written in function of the prior pdf of z , $f(z_0)$ and the conditional pdf's $f(z_0|y_{0,i})$ as:

$$153 \quad f(\mathbf{z}_0 | y_0) \propto \frac{1}{(f(\mathbf{z}_0))^{m-1}} \prod_{j=1}^m f(\mathbf{z}_0 | y_{0,j}) \quad (1)$$

154 If $f(z_0|z_S)$ denotes the pdf of the variable of interest at location \mathbf{x}_0 , solely based on observations
 155 \mathbf{z}_S , obtained through ordinary kriging interpolation of the observation data, if $f(z_0|y_{DEM}(x_0))$
 156 denotes the pdf of z at location \mathbf{x}_0 obtained through an empirical depth-distance relationship
 157 evaluated at \mathbf{x}_0 and if $f(z_0|y_{GW}(x_0))$ is the pdf of z at \mathbf{x}_0 from the estimate of the analytical

158 element groundwater model for location \mathbf{x}_0 , eq. 1 can be written as (cfr. Fasbender *et al.*,
159 2008):

$$160 \quad f(\mathbf{z}_0 | \mathbf{z}_S, y_{DEM}(\mathbf{x}_0), y_{GW}(\mathbf{x}_0)) \propto \frac{f(\mathbf{z}_0 | \mathbf{z}_S)}{f(\mathbf{z}_0)^2} f(\mathbf{z}_0 | y_{DEM}(\mathbf{x}_0)) f(\mathbf{z}_0 | y_{GW}(\mathbf{x}_0)) \quad (2)$$

161 Under the assumption that $f(\mathbf{z}_0)$, $f(\mathbf{z}_0 | \mathbf{z}_S)$, $f(\mathbf{z}_0 | y_{DEM}(\mathbf{x}_0))$ and $f(\mathbf{z}_0 | y_{GW}(\mathbf{x}_0))$ are Gaussian
162 distributed, the posterior pdf $f(\mathbf{z}_0 | \mathbf{z}_S, y_{DEM}(\mathbf{x}_0), y_{GW}(\mathbf{x}_0))$ is also Gaussian. A Gaussian distribution
163 with mean μ and variance σ^2 is given by:

$$164 \quad f(x) = \frac{1}{\sqrt{2\pi\sigma}} \exp\left(-\frac{1}{2\sigma^2}(x-\mu)^2\right) \\ \propto \exp\left(-\frac{1}{2\sigma^2}x^2 + \frac{\mu}{\sigma^2}x\right) \quad (3)$$

165 Replacing the pdf's on the right hand side in eq. 2 by eq. 3, results in the equivalence given by
166 eq. 3:

$$167 \quad f(\mathbf{z}_0 | \mathbf{z}_S, y_{DEM}(\mathbf{x}_0), y_{GW}(\mathbf{x}_0)) \propto \exp\left(\frac{1}{\sigma_0^2}z_0^2 - 2\frac{\mu_0}{\sigma_0^2}z_0\right) \exp\left(-\frac{1}{2\sigma_k^2}z_0^2 + \frac{\mu_k}{\sigma_k^2}z_0\right) \times \\ \exp\left(-\frac{1}{2\sigma_{DEM}^2}z_0^2 + \frac{\mu_{DEM}}{\sigma_{DEM}^2}z_0\right) \exp\left(-\frac{1}{2\sigma_{GW}^2}z_0^2 + \frac{\mu_{GW}}{\sigma_{GW}^2}z_0\right) \quad (4) \\ \propto \exp\left(-\frac{1}{2}\left(\frac{1}{\sigma_k^2} + \frac{1}{\sigma_{DEM}^2} + \frac{1}{\sigma_{GW}^2} - \frac{2}{\sigma_0^2}\right)z_0^2 + \left(\frac{\mu_k}{\sigma_k^2} + \frac{\mu_{DEM}}{\sigma_{DEM}^2} + \frac{\mu_{GW}}{\sigma_{GW}^2} - 2\frac{\mu_0}{\sigma_0^2}\right)z_0\right)$$

168 In eq. 4 μ_0 and σ_0^2 denote the mean and variance of the observed data set, characterizing the
169 prior pdf, μ_k and σ_k^2 the mean and variance of the kriging interpolation, μ_{DEM} and σ_{DEM}^2 the
170 mean and variance of the empirical depth-distance relationship and μ_{GW} and σ_{GW}^2 are the
171 mean and variance of the analytic element groundwater model.

172 Since the conditional probability density function itself is also a Gaussian distribution, the
173 mean and the variance of this pdf, resp. μ_{BDF} and σ_{BDF}^2 , are obtained through equivalence from
174 eq. 4;

$$\left\{ \begin{array}{l} \mu_{BDF} = \left(\frac{\mu_k}{\sigma_k^2} + \frac{\mu_{DEM}}{\sigma_{DEM}^2} + \frac{\mu_{GW}}{\sigma_{GW}^2} - 2 \frac{\mu_0}{\sigma_0^2} \right) \sigma_{BDF}^2 \\ \sigma_{BDF}^2 = \left(\frac{1}{\sigma_k^2} + \frac{1}{\sigma_{DEM}^2} + \frac{1}{\sigma_{GW}^2} - \frac{2}{\sigma_0^2} \right)^{-1} \end{array} \right. \quad (5)$$

175
176 Equation 5 thus provides an elegant and compact formula to estimate a quantity at
177 unmeasured locations by combining a kriging interpolation with different additional data
178 sources, which are exhaustively known in space, with the result of a kriging interpolation.

179 3. Application

180 3.1 Study Area

181 The study area is located in Central Belgium where the geology is dominated by the Brussels
182 Sands Formation (Fig. 1), one of the main aquifers in Belgium for drinking water production.
183 This Brussels Sands aquifer is of Middle Eocene age and consists of a heterogeneous
184 alteration of calcified and silicified coarse sands (Laga et al., 2001). These sands are
185 deposited on top of a clay formation of Early Eocene age, the Kortrijk Formation, which
186 forms the base of the aquifer in the northern part of the study area. In the south, the Kortrijk
187 formation is locally eroded and the Brussels Sands are deposited on top of Paleocene sandy
188 silts (Hannut Formation), Cretaceous chalk deposits (Gulpen Formation) and, mainly,
189 Paleozoic basement rocks consisting of weathered and fractured shales and quartzites. On the
190 hilltops, younger sandy formations of Late Eocene (Maldegem Formation) to Early Oligocene
191 age (St. Huibrechts Hern Formation) cover the Brussels Sands. The latter mainly consist of
192 glauconiferous fine sands. In the north of the study area isolated patches of Oligocene clay,
193 the Boom Formation, and Miocene sands (Diest Formation) occur. The entire study area is
194 covered with an eolian loess deposit of Quaternary age; in the north east of the study area,
195 these loess deposits are more sandy.

196 The main river in the study area is the Dijle River and many of its tributaries have cut through
197 the Brussels Sands during the Quaternary. In most of the valley floors, the Brussels Sands are

198 absent and the unconfined aquifer is situated in alluvial deposits of the rivers on top of the
199 Kortrijk formation. These alluvial deposits consist of gravel at the base, covered with an
200 alteration of silt, sand and peat. In the river valleys, a great number of springs drain the
201 aquifer and provide the base flow for the river Dijle and its tributaries.
202 The hydraulic conductivity of the Brussels Sands varies between 6.9×10^{-5} m/s and 2.3×10^{-4}
203 m/s, because of the heterogeneity of the Eocene aquifer (Bronckers and De Smedt, 1991).
204 Locally, in the alluvial gravels, higher conductivities are observed with values as high as $9.3 \times$
205 10^{-4} m/s. Small scale sedimentary structures have been proven to influence permeability
206 (Huysmans et al., 2008).
207 Both the Flemish (DOV, 2009) and Walloon government (DGRNE, 2009) have observation
208 wells installed in the Brussels Sands aquifer to monitor groundwater level fluctuations and
209 groundwater chemistry. 176 groundwater head observations from these monitoring networks
210 are used for water table interpolation. The location of the observation wells, the river network
211 and the topography is indicated in figure 2.

212 **3.2 Ordinary Kriging**

213 Since the river Dijle drains towards the north and topography declines in that direction, the
214 head observation data display a clear north-south trend (Fig. 3a). A linear trend is fitted to the
215 data and removed from the data before calculating the experimental variogram (Fig. 3b). The
216 experimental variogram is modeled, by fitting in a least-squares sense, with a Gaussian
217 variogram with a nugget of 11 m^2 , a sill of 308 m^2 and range of 11170 m (Fig. 3b).
218 Ordinary kriging with a trend in the Y-direction, based on the original data and the
219 experimental variogram, is performed on a regular grid with grid cell size of 50 m , having
220 1140 rows and 1060 columns. In order to incorporate the anisotropy induced by the presence
221 of the draining Dijle-River the main axis of the search ellipsoid is oriented N12E. The radii of
222 the ellipse are 50000 m and 20000 m with a maximum number of 75 conditioning data.

223 Kriging is performed using the Stanford Geostatistical Modeling Software (S-GeMS, Remy,
 224 2004). The kriging interpolation of groundwater head is depicted in figure 5a, the associated
 225 variance in figure 5b.

226 3.3 Empirical depth-distance relationship

227 In a first attempt to include additional information in water table spatial mapping within the
 228 Bayesian Data Fusion framework, Fasbender *et al.* (2008) used a Digital Elevation Model and
 229 the geometry of the river network. In an aquifer with a draining hydrographic network, water
 230 table elevations are expected to be in close proximity to ground surface near the river
 231 network. In an unconfined aquifer, recharge will lead to groundwater mounding in the
 232 interfluves. Compared to the rise in elevation of ground level on the interfluves, this
 233 mounding generally is rather low, especially in highly conductive aquifers. Fasbender *et al.*
 234 (2008) therefore postulate that it is possible to find an empirical functional that relates the
 235 DEM value to the groundwater level at a certain location based on the distance of the location
 236 to the river network. This relationship can be expressed as:

$$\begin{aligned}
 237 \quad Z(x_i) &= y_{DEM}(x_i) + E(x_i) \\
 y_{DEM}(x_i) &= DEM(x_i) - g(d_{DEM}(x_i))
 \end{aligned}
 \tag{6}$$

238 where $Z(x_i)$ is the water table elevation, $y_{DEM}(x_i)$ is the empirical functional and $E(x_i)$ is a zero-
 239 mean random error with a variance σ_{DEM}^2 . $DEM(x_i)$ is the DEM-value at location x_i , $d_{DEM}(x_i)$
 240 is the penalized distance of x_i to the nearest point on the river network and $g()$ is an increasing
 241 nonnegative function. The variance σ_{DEM}^2 increases with increasing $d_{DEM}(x_i)$. This reflects a
 242 weakening of the correspondence between water table elevation and ground level elevation as
 243 the distance to the river network increases. The distance calculation between x_i and the river
 244 network is penalized by using the slope of the terrain. In areas in which the valleys have steep
 245 slopes, a relationship between ground level elevation and water table elevation will not be
 246 justified, even if the Euclidean distance to the river network is small. In areas with wide

247 valley floors on the other hand, water tables will be close to ground level, even if the
248 Euclidean distance to the river network is large. By incorporating the slope in the distance
249 calculation, areas with high ground level fluctuations will have high $d_{DEM}(x_i)$ values and
250 associated high σ_{DEM}^2 -values, ensuring that these areas will get less credit in the BDF model.
251 For each observation location the penalized distance to the nearest point on the hydrographic
252 network is calculated together with the depth of the water table (Fig. 4). The depth to water
253 table clearly increases with increasing penalized distance, especially for relatively small
254 penalized distances. With higher penalized distance, the relationship is not readily apparent. A
255 logistic-like functional $g()$ is fitted based on these observations and a same logistic-like
256 equation is used to model the variance of $E(x_i)$. The choice of a logistic-like functional is
257 motivated as it allows an increase of depth with increasing distance, while reaching a plateau
258 for larger distances. Using the same type of equation for the variance σ_{DEM}^2 , ensures that with
259 increasing distance, the variance increases and the influence of the depth-distance relationship
260 on the BDF-result decreases.
261 The water table estimate by the empirical depth-distance relationship is shown in figure 5c
262 and the associated variance in figure 5d.

263 **3.4 Analytic Element Groundwater Model**

264 The analytic element method represents aquifer features by points, line sinks and area-sinks
265 which can be head or discharge-specified to model groundwater flow (Strack, 2003). As the
266 solution to the groundwater flow equations is obtained by superimposing functions of
267 complex potentials representing the aquifer features, there is no need to discretise the flow
268 domain or specify boundary conditions at the perimeter of the model domain as is needed for
269 finite-difference and finite-element models (Strack, 2003). Additionally, representing aquifer
270 features by analytic elements facilitates the numerical implementation of the method in
271 object-oriented programming languages (Bakker and Kelson, 2009). Seeing the relative ease

272 of implementing analytic element models, they are popular as a hydrologic screening tool
 273 (Hunt, 2006). Karanovic *et al.* (2009) use solutions of analytic elements as drift terms in
 274 kriging groundwater heads in an area subject to pumping.

275 In this study an analytic element groundwater model is created for the Brussels Sands aquifer,
 276 using the Tim^{ML}-code (Bakker and Strack, 2003). It serves as secondary information in the
 277 Bayesian Data Fusion. The aquifer is represented by a single, unconfined layer with a uniform
 278 hydraulic conductivity. The river network shown in figure 2 is implemented as prescribed
 279 head line-sinks with a head elevation derived from the DEM. A constant, uniform infiltration
 280 of 300 mm/year (Batelaan *et al.*, 2003) is assigned to the model through a rectangular
 281 infiltration area equal to the area spanned by the bounding box of figure 2. The base of the
 282 layer is set to -25 m asl and is assumed to be constant. This is the most simplifying step in the
 283 conceptualization of the groundwater flow system, as it is known that the base of the aquifer
 284 is irregular, slopes towards the north and varies between 140 m asl in the south and -70 m asl
 285 in the north of the study area (Cools *et al.* 2006). The value of -25 m asl is chosen to ensure
 286 the base of the aquifer is well below the specified head values at the line sinks throughout the
 287 flow domain.

288 A sensitivity analysis with regards to the base level of the aquifer, hydraulic conductivity and
 289 recharge rate is carried out using UCODE (Poeter *et al.*, 2005). The composite scaled
 290 sensitivity (css) is used to evaluate the parameter sensitivity and is defined as (Hill and
 291 Tiedeman, 2007):

$$292 \quad \text{css} = \sum_{i=1}^n \sqrt{\frac{1}{n} \left(\left(\frac{\partial h_i'}{\partial b} \right) |b| \right)^2} \quad (7)$$

293 with $\frac{\partial h_i'}{\partial b}$ the sensitivity of the simulated value h'_i associated with the i -th observation with
 294 respect to parameter b . Using the head observations from section 3.1, the composite scaled

295 sensitivity of recharge rate and hydraulic conductivity are 0.33 and 0.32 respectively, while
 296 the value for the base of the aquifer is much lower, 8.1×10^{-3} .

297 The analytic element model is automatically calibrated by changing the hydraulic
 298 conductivity. Recharge rate is not changed, as changes in this parameter are correlated to
 299 changes in the hydraulic conductivity parameter. The effect of an increase in recharge rate on
 300 hydraulic heads in the aquifer can be countered by increasing the hydraulic conductivity. In a
 301 situation as outlined above with an unconfined aquifer with a single hydraulic conductivity
 302 and recharge rate, a unique solution to the parameter optimization can not be obtained by
 303 simultaneously changing both parameters (Hill and Tiedeman, 2007). The final hydraulic
 304 conductivity obtained after calibration is 1.74×10^{-6} m/s. As could be expected, this value is
 305 an order of magnitude lower than the values from pumping tests since the base of the aquifer
 306 is underestimated.

307 As for the empirical depth-distance relationship, the estimated groundwater level, $y_{GW}(x_i)$, at a
 308 location x_i , can be related to the unknown, true groundwater level $Z(x_i)$ by addition of an error
 309 term $E(x_i)$ with a zero-mean and a variance σ_{GW}^2 :

$$310 \quad Z(x_i) = y_{GW}(x_i) + E(x_i) \quad (8)$$

311 The variance is chosen to be uniform throughout the model domain, and in order to reflect the
 312 capability of the analytic element model at simulating groundwater levels, the mean squared
 313 error between observed and simulated head is used to model the variance

$$314 \quad \sigma_{GW}^2 = \frac{1}{N} \sum_{i=1}^N \hat{e}_i^2 \quad (9)$$

315 where \hat{e}_i is the estimated error at location x_i and N equal to 176. The estimated groundwater
 316 level using the calibrated analytic element model is shown in figure 5c and the associated
 317 variance in figure 5d.

318 By using more elaborate conceptual models, more closely reflecting the spatial variability in
 319 recharge, hydraulic conductivity and base of the aquifer, it is not unlikely that the estimated
 320 variance will decrease and the influence of the groundwater model on the final BDF
 321 interpolation would increase. This would however be beyond the scope of the methodology,
 322 which aims at providing an interpolation methodology using limited information on the
 323 aquifer properties.

324 **3.5 Bayesian Data Fusion**

325 The Bayesian Data Fusion outlined in section 2 is applied to the study area. In order to asses
 326 and to compare the influence of the different additional data sources, three different BDF
 327 interpolations are carried out, combining (1) kriging with the empirical depth-distance
 328 relationship, (2) kriging with the analytical element groundwater model and finally (3) kriging
 329 with the empirical depth-distance relationship and the analytical element groundwater model.
 330 The former can be implemented by using eq. 5. For the first interpolation, eq. 5 simplifies to:

$$331 \quad \mu_{BDF} = \left(\frac{\mu_k}{\sigma_k^2} + \frac{\mu_{DEM}}{\sigma_{DEM}^2} - \frac{\mu_0}{\sigma_0^2} \right) \sigma_{BDF}^2 \quad (10)$$

$$\sigma_{BDF}^2 = \left(\frac{1}{\sigma_k^2} + \frac{1}{\sigma_{DEM}^2} - \frac{1}{\sigma_0^2} \right)^{-1}$$

332 A similar equation can be found for the BDF combining kriging with the analytic element
 333 model.

334 The interpolated head obtained through the different BDF interpolations and the associated
 335 variances are shown in figure 6.

336 To asses the predictive capability of the proposed methodology and to compare the different
 337 Bayesian Data Fusion results to each other and to the individual secondary data sources, a
 338 ‘leave-one-out’ cross-validation as outlined by Chilès and Delfiner (1999, p. 111) is carried
 339 out. For each observation location x_0 groundwater level and associated variance is calculated
 340 based on the surrounding observations, without taking into account the observed groundwater

341 level at location x_0 . The obtained results are compared to the observed groundwater levels by
 342 means of scatter plots and by calculating the root mean squared error (RMSE) and normalized
 343 root mean squared error (NRMSE) according to

$$\begin{aligned}
 344 \quad RMSE &= \sqrt{\frac{1}{N} \sum_{i=1}^N \hat{e}_i^2} \\
 NRMSE &= \frac{RMSE}{\max(h_{obs}) - \min(h_{obs})}
 \end{aligned} \tag{11}$$

345 with \hat{e}_i the estimated error at location x_i and N the number of observations h_{obs} . The
 346 calculated RMSE and NRMSE are given in table 1.
 347 For the kriging interpolation, cross-validation consisted of estimating groundwater level and
 348 variance at observation location x_i without taking into account the groundwater level
 349 observation at x_i . For the cross-validation of the empirical depth-distance relationship, the
 350 relationship and associated variance is estimated without using the observation at x_i . As such,
 351 the analytic element model does not use the observations to estimate groundwater level. The
 352 calculated groundwater level at location x_i is therefore used as a cross-validation value. The
 353 associated variance however, obtained through eq. 9, is calculated without using the
 354 groundwater level observation at x_i .
 355 The cross-validation of the three BDF interpolations at x_i is obtained by plugging the
 356 groundwater level and variance at x_i from the cross-validation of the secondary information
 357 sources, into eq. 5 and 10.

358 **4. Discussion**

359 From Figure 5a it is apparent that kriging produces a smoothly varying water table contour
 360 map with depressions situated in the vicinity of the major rivers (Fig. 2). The variance map
 361 (Fig. 5b) however shows the irregular distribution of observation points and the resulting low
 362 variance in the central area with a high observation density, while the eastern and western
 363 borders, regions scarce of data, are characterized by a high variance. This variance map helps

364 to explain a number of interpolation artifacts present in Figure 5a. In regions in the vicinity of
365 (x,y)-coordinates (170000,165000) and (x,y)-coordinates (147000,145000), isolated
366 depressions are interpolated. Such depressions should only occur in a groundwater level
367 contour map if a groundwater extraction, by pumping wells or evaporation through a pond, is
368 present. In this aquifer system however the depression represents a part of the flow
369 convergence due to the draining influence of the river network. In regions with low data-
370 density, like the south-east around (x,y)-coordinates (180000,150000), the search ellipsoid
371 will not contain enough observation points to produce a reliable interpolation. The contour
372 lines can therefore locally have a jagged appearance although a Gaussian variogram model is
373 used. In a water table interpolation, jagged contour lines should not appear since groundwater
374 levels are to be considered a spatially smoothly varying quantity.

375 The cross-validation (Fig. 7a) shows that the residuals are centered on zero and, although
376 some outlying residuals show a considerable departure from zero, the root mean squared error
377 is only 7.24 m and the normalized root mean squared error 4.99 %.

378 The RMSE and NRMSE of the calibrated analytical element groundwater model are
379 comparable to the result of kriging (Table 1). The scatterplot of observed vs calculated values
380 (Fig. 7b) however shows that although the number of very large residuals is smaller compared
381 to kriging, the spread of the residuals around zero is larger. In the groundwater level map
382 (Fig. 5c) the difference between the analytic element groundwater model and kriging is
383 clearly visible. The groundwater map shows the draining influence near the rivers and the
384 groundwater mounding due to groundwater recharge in the interfluves. Although the shape of
385 the water table more closely reflects the hydrogeological information available of the aquifer
386 system, locally sizeable differences between observed and calculated groundwater levels
387 exist.

388 The groundwater level estimated by the empirical depth-distance relationship can be
389 considered a subdued replica of topography. On the interfluves, the contour lines are irregular,
390 reflecting variations in the DEM, while the groundwater levels at these locations are expected
391 to be rather smooth and gradually changing. These zones are assigned a high variance, as they
392 have a large penalized distance to the river network. In zones with a low relief, like the
393 alluvial plains and the northern part of the study area, groundwater levels are estimated close
394 to ground surface. The predictive abilities of this empirical model (table 1 and fig. 7c) appear
395 to be only slightly lower than these of kriging interpolation.

396 The first result of Bayesian Data Fusion interpolation is the combination of the kriging
397 interpolation with the estimate from the empirical depth-distance relationship, as already
398 implemented by Fasbender *et al.* (2008). In the areas with low relief smooth contour lines are
399 produced (Fig. 6a) and the drainage network is incorporated in the interpolation result. On the
400 interfluves however, the contour lines are often highly irregular with numerous small isolated
401 groundwater mounds and depressions. The variance map (Fig. 6b) shows that the zones with
402 high data density and low relief have low variance values. These values increase rapidly
403 however in zones with considerable relief and low data density. The scatterplot of cross-
404 validation results (Fig. 7e) and the RMSE value of 4.91m (Table 1) indicate a marked
405 improvement in predictive capability, compared to the individual additional data sources.

406 The BDF interpolation combining kriging with the analytic element groundwater model (Fig.
407 6c), shows a contour map which is similar to the contour map of the analytic element
408 groundwater model (Fig. 5c). The AEM groundwater model however appears to locally
409 overestimate the amount of groundwater mounding in the interfluves. This is remediated in
410 zones with high data density, like around x,y-coordinates (170000,170000), by the higher
411 weight of the kriging in the interpolation. In zones with low data density, the effect of the
412 drainage network on the contour lines of groundwater elevation is clearly apparent. Where

413 data density is high in the vicinity of a river, it is possible that kriging dominates the
414 interpolation as can be seen near x,y-coordinates (145000,150000) and x,y-coordinates
415 (160000,160000). As the AEM groundwater model is characterized by a uniform variance,
416 the variance of BDF of the kriging and AEM (Fig. 6d) is a scaled replica of the kriging
417 variance (Fig. 5b). The RMSE of this interpolation, 5.42 m, is slightly higher than the RMSE
418 of the BDF of kriging and the depth-distance relationship. The main reason for the higher
419 RMSE is the presence of higher residuals for the observations with groundwater levels above
420 100m, while for observations below 100m the BDF of kriging and AEM has lower residuals.
421 The ultimate interpolation combines the three data sources, kriging, depth-distance
422 relationship and AEM groundwater model (Fig. 6e). The general shape of the contour lines is
423 largely influenced by the analytic element model. Locally the influence of the other data
424 sources is apparent, especially in zones with high data density (kriging) and near the river
425 network (depth-distance relationship). The influence of the depth-distance relationship can
426 also be seen on the interfluves through the irregularities in the contour lines, arising from
427 the DEM-fluctuations. The variance of the BDF in Fig. 6f benefits clearly from incorporating
428 the empirical depth-distance relationship. The cross-validation results, i.e. both the scatterplot
429 and the RMSE value, show that the combination of the three data sources has the highest
430 predictive capabilities.

431 **Conclusions**

432 The water table interpolation methodology introduced by Fasbender et al. (2008), based on
433 the Bayesian Data Fusion framework (Bogaert and Fasbender, 2007), is further extended to
434 incorporate conceptual hydrogeological information through groundwater head calculation
435 based on an analytic element groundwater model.

436 The methodology is applied to a sandy aquifer in Belgium using a limited number of head
437 observations. The Bayesian Data Fusion methodology is used to combine kriging with an

438 estimate of groundwater level by an empirical depth-distance relationship and a groundwater
439 level estimate from an automatically calibrated analytic element model.

440 Combining kriging with the empirical depth-distance relationships produces reliable results in
441 areas with low relief and close to the river network. The estimate in zones scarce of data,
442 farther away from the river network benefits from combining the kriging with the analytic
443 element groundwater model. Combining the three sources of data results in a groundwater
444 level interpolation with a high level of predictive capabilities as shown through the leave-one-
445 out cross-validation, albeit that the shape of the contour lines in the interfluves can be
446 debatable by the presence of irregularities arising from contribution of the depth-distance
447 relationship.

448 The interpolation methodology presented and applied in this paper shows that using different
449 sources of data in groundwater interpolation within the Bayesian Data Fusion framework,
450 even with limited data, it is possible to produce an accurate water table contour map
451 incorporating conceptual hydrogeological information.

452 **Acknowledgements**

453 The authors would like to express their gratitude towards DOV and DGRNE for providing the
454 groundwater level observations for the Flemish and Walloon part of Belgium respectively.

455 The comments of the three anonymous reviewers are highly valued and contributed greatly to
456 the improvement of this paper.

457 **References**

- 458 Bakker, M. and V.A. Kelson (2009) Writing analytic element programs in Python. *Ground*
459 *Water* 47 (6) 828-834 doi: 10.1111/j.1745-6584.2009.00583.x
- 460 Bakker, M. and O.D.L. Strack (2003) Analytic elements for multiaquifer flow. *Journal of*
461 *Hydrology* 271 (1-4) 119-129
- 462 Batelaan, O., De Smedt, F. and L. Triest (2003) Regional groundwater discharge:
463 phreatophyte mapping, groundwater modeling and impact analysis of land-use change.
464 *Journal of Hydrology* 275 (1-2) 86-108 doi: 10.1016/S0022-1694(03)00018-0
- 465 Bogaert, P. and D. Fasbender (2007), Bayesian data fusion in a spatial prediction context: a
466 general formulation. *Stochastic Environmental Research And Risk Assessment* 21 (6)
467 695-709, doi: 10.1007/s00477-006-0080-3
- 468 Bronders, J. and F. De Smedt (1991) Geostatistische analyse van de hydraulische
469 geleidbaarheid van watervoerende lagen in Midden-België. (*Geostatistical analysis of*
470 *hydraulic conductivity of the aquifers in Central Belgium, in Dutch*). *Water* 59 (4) 127-
471 132
- 472 Buchanan, S. and J. Triantafilis (2009) Mapping water table depth using geophysical and
473 environmental variables. *Ground Water* 47 (1) 80-96, doi: 10.1111/j.1745-
474 6584.2008.00490
- 475 Chilès, J.-P. and P. Delfiner (1999) *Geostatistics: modeling spatial uncertainty*. Wiley: New
476 York
- 477 Cools, J., Meyus, Y., Woldeamlak, S. T., Batelaan, O. and F. De Smedt (2006) Large-scale
478 GIS-based hydrogeological modelling of Flanders: a tool for groundwater management.
479 *Environmental Geology* 50 (8) 1201-1209, doi: 10.1007/s00254-006-0292-3
- 480 Cressie, N. and C.K. Wikle (2002) Space-time Kalman filter. In: El-Shaarawi, A. H. and W.
481 W. Piegorisch (eds). *Encyclopedia of Environmetrics. Vol. 4*. 2045-2049. Wiley.

- 482 Databank Ondergrond Vlaanderen (DOV) (2009) Puntenlaag grondwatermeetnet. (*Subsoil*
483 *Database Flanders, Point layer groundwater observation network, in Dutch*) Consulted
484 25 May 2009, at <http://dov.vlaanderen.be>
- 485 Direction Générale des Ressources Naturelles et de l'Environnement (DGRNE) (2009),
486 Banque de données 10-sous. (*Database 10-sous, in French*)
- 487 Desbarats, A. J., Logan, C. E., Hinton, M. J. and D.R. Sharpe (2002) On the kriging of water
488 table elevations using collateral information from a digital elevation model. *Journal of*
489 *Hydrology* 255 (1-4) 25-38, doi:10.1016/S0022-1694(01)00504-2
- 490 Ehrendorfer, M. (2007) A review of issues in ensemble-based Kalman filtering.
491 *Meteorologische Zeitschrift* 16 (6) 795-818, doi:10.1127/0941-2948/2007/0256
- 492 Fasbender, D., Peeters, L., Bogaert, P. and A. Dassargues (2008) Bayesian data fusion applied
493 to water table spatial mapping. *Water Resources Research* 44 W12422
494 doi:10.1029/2008WR006921
- 495 Haitjema, H. M. and S. Mitchell-Bruker (2005) Are water tables a subdued replica of the
496 topography? *Ground Water* 43 (6) 781-786 doi:10.1111/j.1745-6584.2005.00090
- 497 Hill, M. C. and Tiedeman, C. R. (2007) *Effective groundwater model calibration*. Wiley
- 498 Hunt, R.J. (2006) Groundwater modeling applications using the analytic element method.
499 *Ground Water* 44 (1) 5-14 doi:10.1111/j.1745-6584.2005.00143.x
- 500 Huysmans, M., Peeters, L., Moermans, G. and A. Dassargues (2008) Relating small-scale
501 sedimentary structures and permeability in a cross-bedded aquifer. *Journal of Hydrology*
502 361 (1-2) 41-51, doi:10.1016/j.jhydrol.2008.07.047
- 503 Karanovic, M, Tonkin, M and D. Wilson (2009) KT3D_H2O: A program for kriging water
504 level data using hydrologic drift terms. *Ground Water* 47 (4) 580-586
505 doi:10.1111/j.1745-6584.2009.00565.x
- 506 Kresic, N. (2006) *Hydrogeology and groundwater modeling. Second Edition*. CRC Press.

- 507 Laga, P., Louwye, S. and S. Geets (2001) Paleogene and neogene lithostratigraphic units
508 (Belgium). *Geologica Belgica* 4 (1-2) 135-152
- 509 Linde, N., Revil, A., Bolève, A., Dagès, C., Castermant, J., Suski, B. and M. Voltz (2007)
510 Estimation of the water table throughout a catchment using self-potential and
511 piezometric data in a Bayesian framework. *Journal of Hydrology* 334 (1-2) 88-98,
512 doi:10.1016/j.jhydrol.2006.09.027
- 513 Poeter, E., Hill, M.C., Banta, E., Mehl, S. and S. Christensen (2005) UCODE_2005 and six
514 other computer codes for universal sensitivity analysis, calibration and uncertainty
515 evaluation. US Geological Survey Techniques and Methods 6-A11. 283p.
- 516 Procter, C., Comber, L., Betson, M., Buckley, D., Frost, A., Lyons, H., Riding, A. and K.
517 Voyce (2006) Identifying crop vulnerability to groundwater abstraction: Modeling and
518 expert knowledge in a GIS. *Journal of Environmental Management* 81 (3) 296-306,
519 doi:10.1016/j.jenvman.2006.01.016
- 520 Reilly, T. E. (2001) System and boundary conceptualization in groundwater flow simulation.
521 *Techniques of water-resources investigations of the US Geological Survey Book 3,*
522 *applications of Hydraulics, Chapter B8.* US Geological Survey: Virginia
- 523 Rémy, N. (2004) *S-GeMS: Geostatistical Earth Modelling Software: User's Manual.* Stanford
524 University: Stanford
- 525 Rivest, M., Marcotte, D. and P. Pasquier (2008) Hydraulic head field estimation using kriging
526 with an external drift: A way to consider conceptual model information. *Journal of*
527 *Hydrology* 361 (3-4) 349-361, doi:10.1016/j.jhydrol.2008.08.006
- 528 Strack, O.D.L. (2003) Theory and applications of the analytic element method. *Reviews of*
529 *geophysics* 41 (2) 1005 doi:10.1029/2002RG000111
- 530 Sun, Y., Kang, S., Li, F. and L. Zhang (2009) Comparison of interpolation methods for depth
531 to groundwater and its temporal and spatial variations in the Minqin oasis of northwest

- 532 China. *Environmental Modelling & Software* 24 (10) 1163-1170.
- 533 doi:10.1016/j.envsoft.2009.03.009
- 534 Taany, R., Tahboub, A. and G. Saffarini (2009) Geostatistical analysis of spatiotemporal
- 535 variability of groundwater level fluctuations in Amman-Zarqa basin, Jordan: a case
- 536 study. *Environmental Geology* 57 (3) 525-535, doi:10.1007/s00254-008-1322-0
- 537 Tonkin, M. J. and S. P. Larson (2002) Kriging water levels with a regional-linear and point-
- 538 logarithmic drift. *Ground Water* 40 (2) 185-193,

539 **Figure Captions**540 Figure 1: Geological map of the study area (after Cools *et al.*, 2006)

541 Figure 2: Topography of the study area, river network and head observation locations.

542 Figure 3: (a) north-south trend identification from observation data and (b) experimental
 543 variogram together with the Gaussian variogram model (nugget: 11m^2 , sill: 308m^2 ,
 544 range: 11170 m)

545 Figure 4: Graph of groundwater depth $\text{DEM}(x) - Z(x)$ as a function of penalized distance
 546 $d_{\text{DEM}(x)}$ to the network. Dots represent the observed pair of values, solid line
 547 represents the fitted nonlinear relationship $g()$, whereas dashed lines represent the
 548 95% symmetric confidence interval based on a Gaussian distribution.

549 Figure 5: (a) kriging interpolation, (b) kriging variance, (c) groundwater levels from the
 550 analytic element groundwater model, (d) variance of the analytic element
 551 groundwater model, (e) groundwater levels estimated with the empirical depth-
 552 distance relationship (f) variance of the empirical depth-distance estimated
 553 groundwater level

554 Figure 6: (a) BDF of kriging and DEM, (b) variance of BDF of kriging and DEM, (c) BDF of
 555 kriging and AEM, (d) variance of BDF of kriging and AEM, (e) BDF of kriging,
 556 DEM and AEM, (f) variance of BDF of kriging, DEM and AEM.

557 Figure 7: Cross-validation results. Observed vs calculated values by (a) kriging, (b) analytic
 558 element groundwater model, (c) empirical depth-distance relationship, (e) BDF of
 559 kriging and AEM, (f) BDF of kriging and DEM, (e) BDF of kriging, AEM and DEM

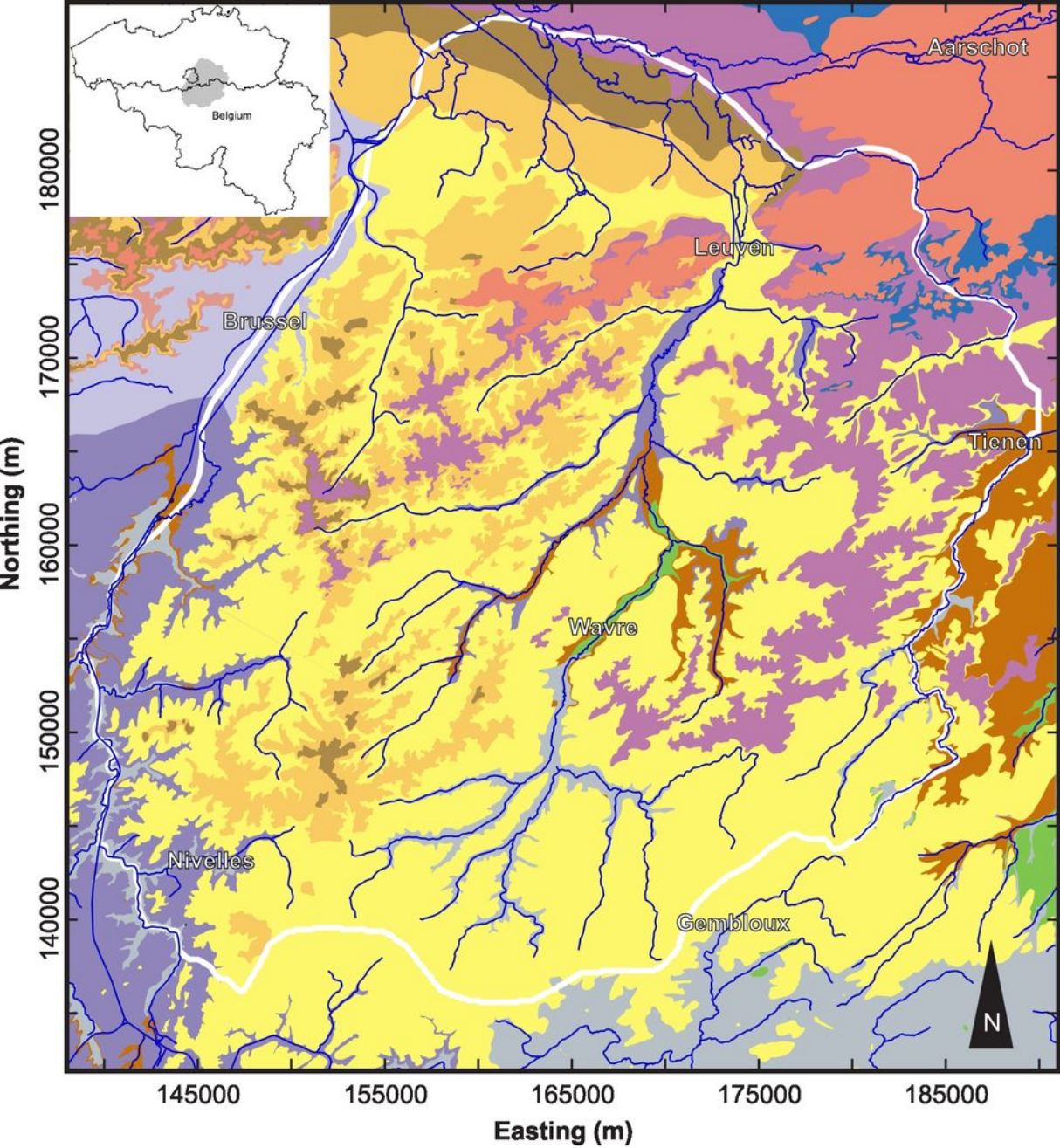
560

561 **Tables**

562 Table 1: Root mean squared error and normalized root mean squared error of cross-validation

Method	RMSE (m)	NRMSE (-)
Kriging	7.24	4.99
AEM	6.57	4.52
DEM	7.37	5.08
BDF Kriging - AEM	5.42	3.73
BDF Kriging - DEM	4.91	3.39
BDF Kriging - AEM - DEM	4.77	3.29

563

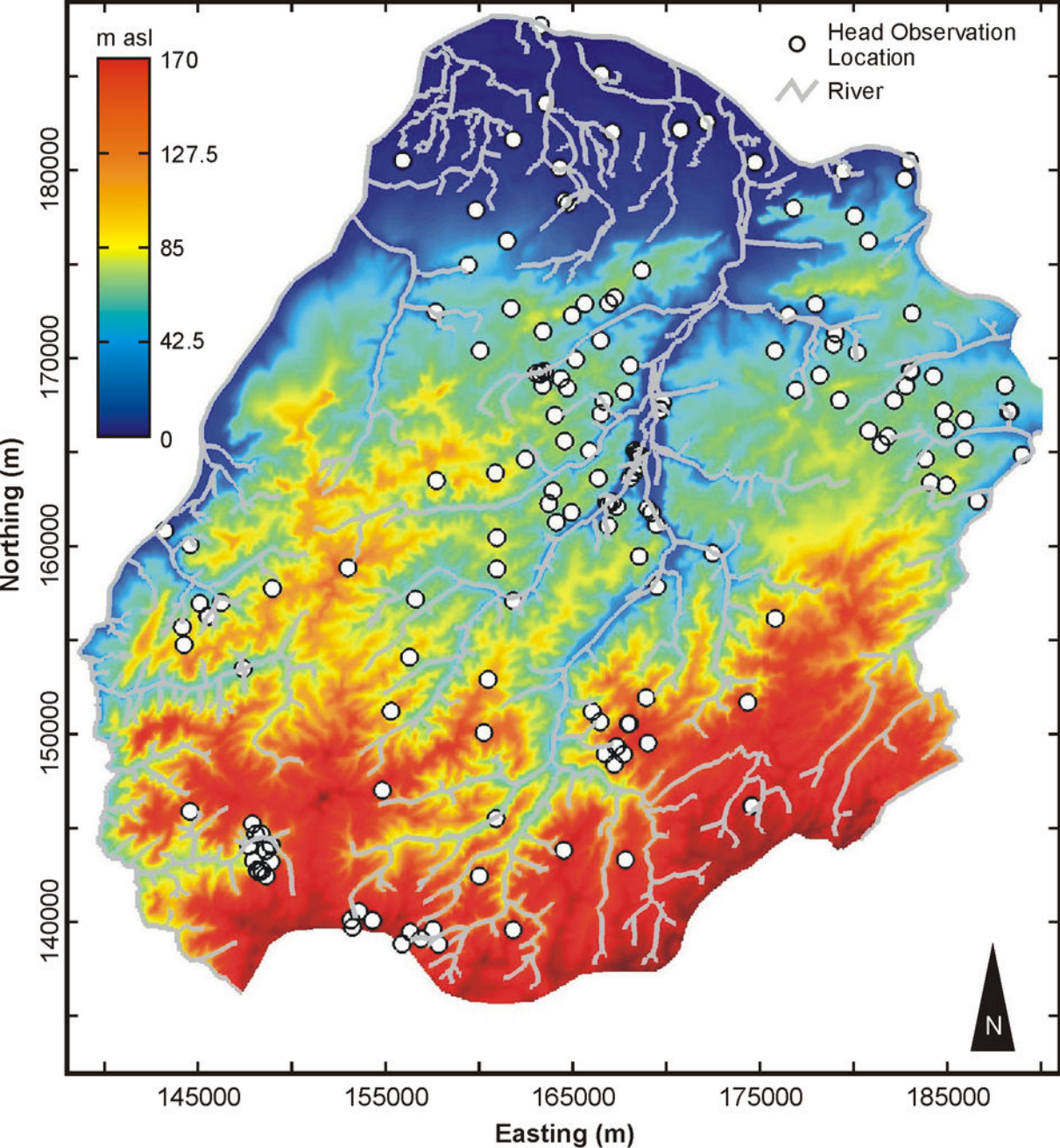


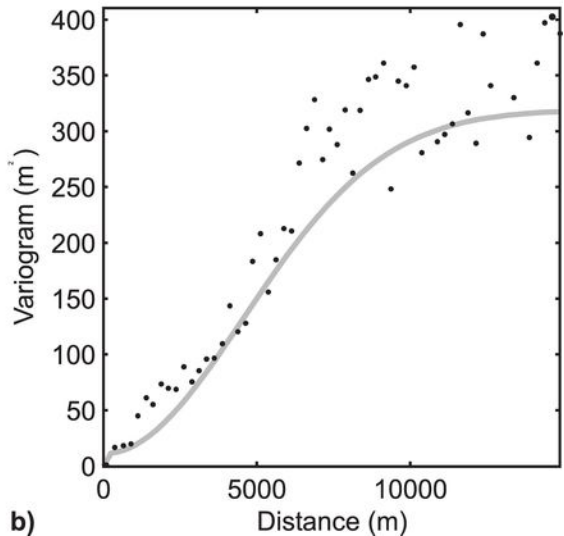
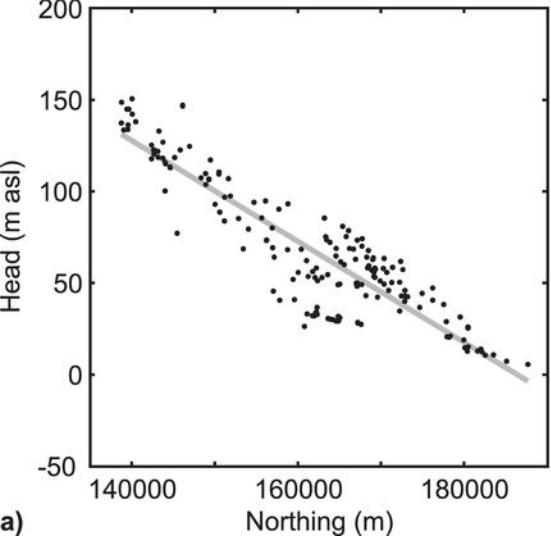
- Miocene Diest Sand
- Oligocene Bolderberg/ Boom/Bilzen/Borgloon Fm
- Oligocene St. H. Hern Sand
- Eocene Maldegem Sand / Clay
- Eocene Lede Sand
- Eocene Brussel Sand

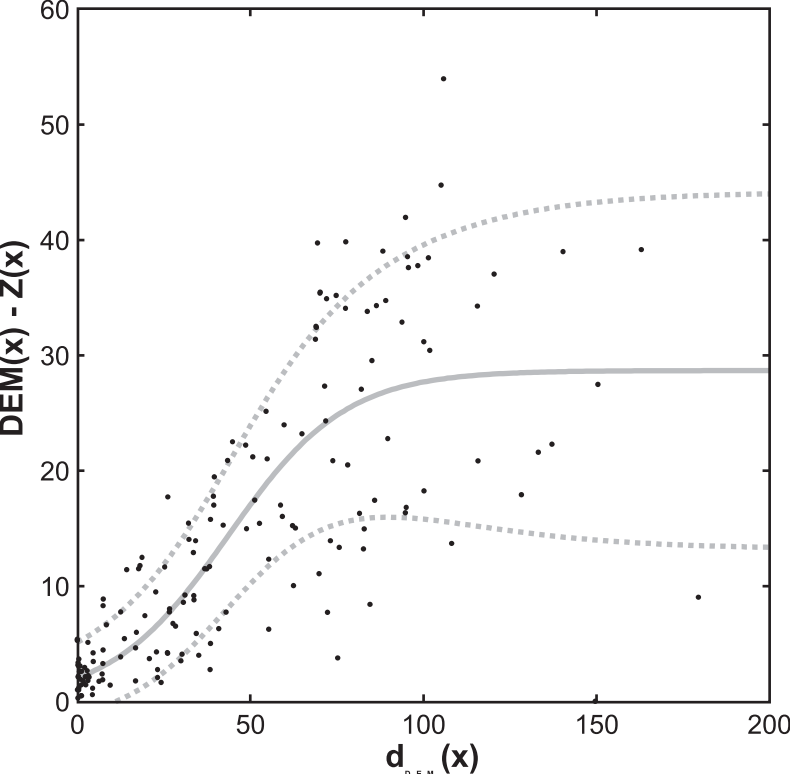
- Eocene Gentbrugge Sand / Clay
- Eocene Tielt Silt / Sand
- Eocene Kortrijk Clay
- Paleocene Hannut Silt / Sand
- Cretaceous Gulpen Chalk
- Paleozoic Basement Quartzite / Shale

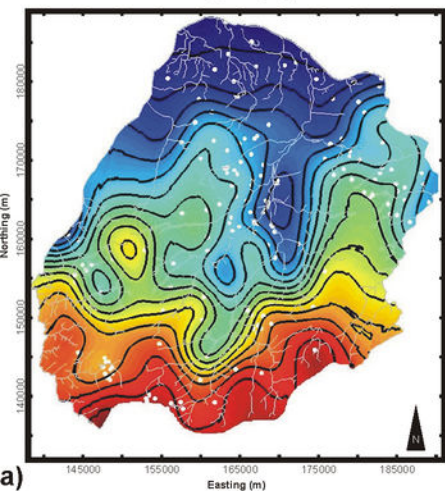
Rivers
 Study Area

0 5 10
 km

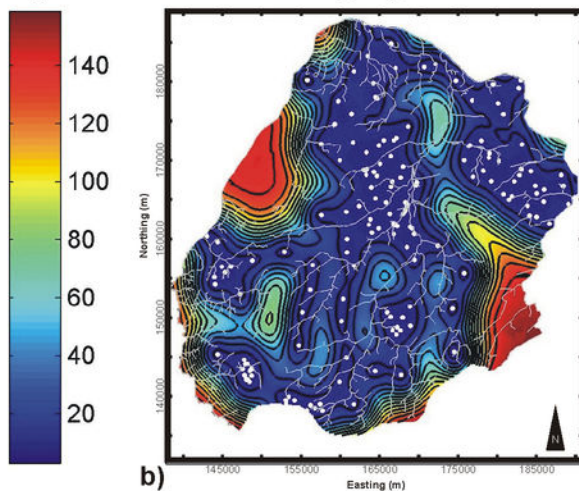






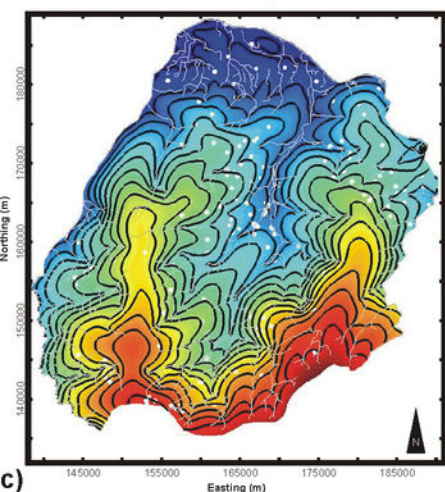
Kriging μ 

m

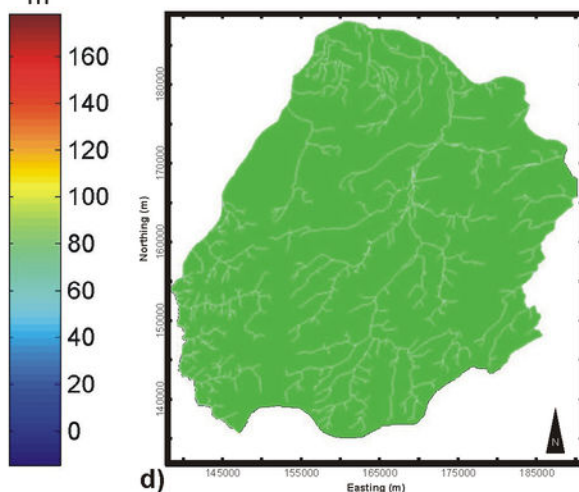
Kriging σ^2  m^2

a)

b)

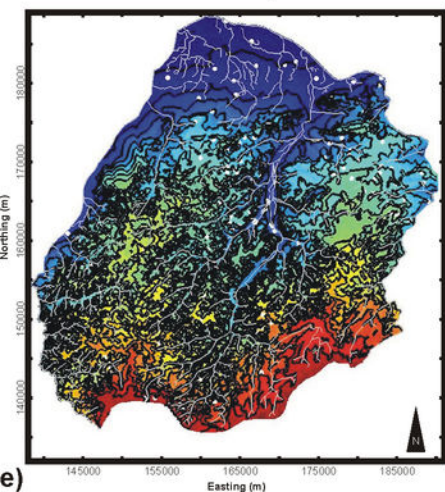
AEM μ 

m

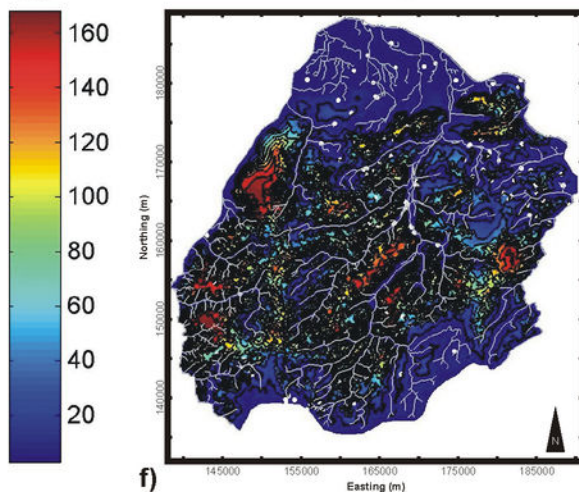
AEM σ^2  m^2

c)

d)

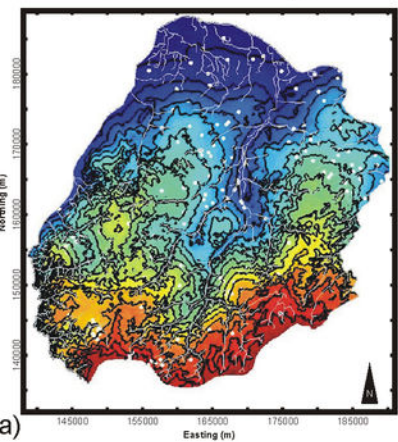
DEM μ 

m

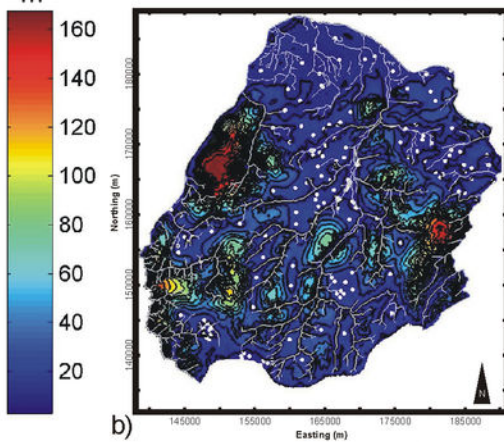
DEM σ^2  m^2

e)

f)

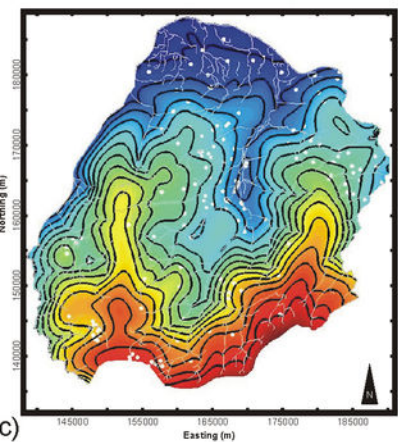
BDF K-DEM μ 

m

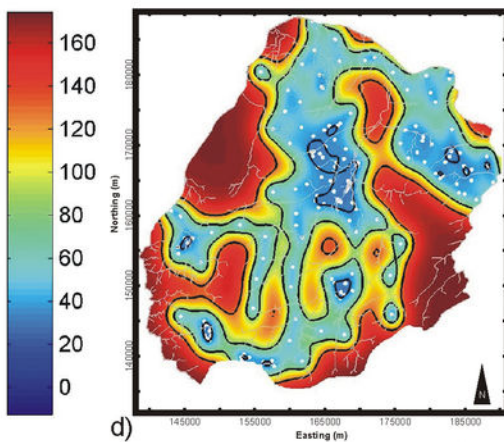
BDF K-DEM σ^2  m^2

a)

b)

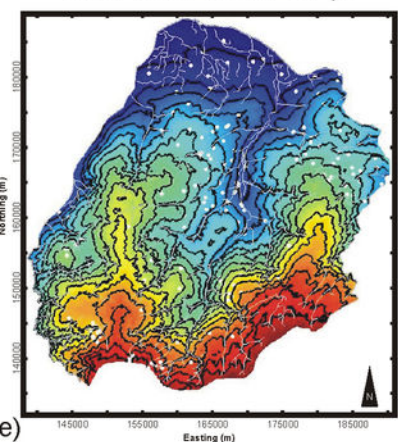
BDF K-AEM μ 

m

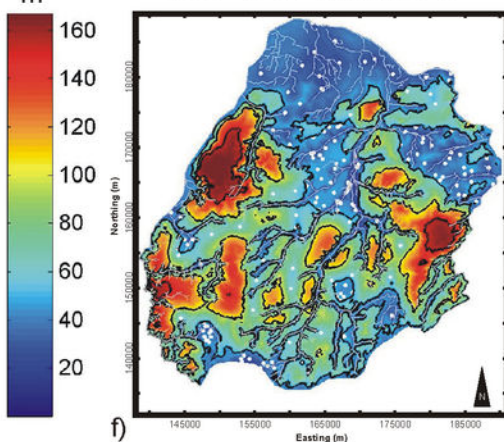
BDF K-AEM σ^2  m^2

c)

d)

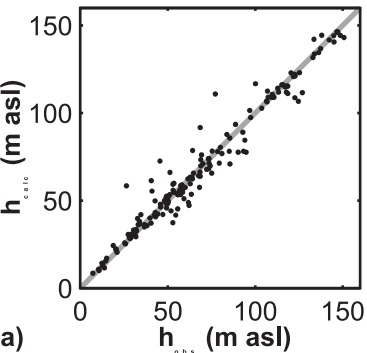
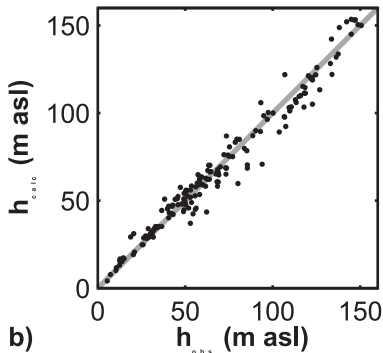
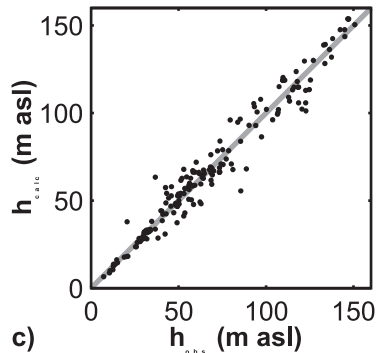
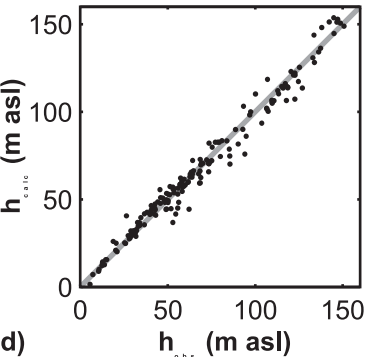
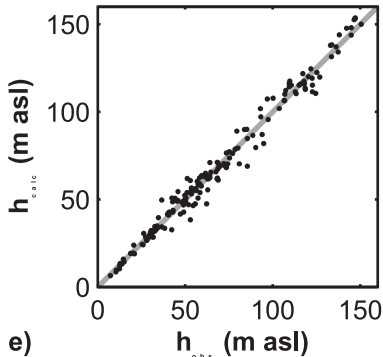
BDF K-DEM-AEM μ 

m

BDF K-DEM-AEM σ^2  m^2

e)

f)

Kriging**AEM****DEM****BDF K-AEM****BDF K-DEM****BDF K-AEM-DEM**